Magnetic Pulse Welding of Sheets – Process Modelling

R. Shotri[1*], G. Racineux[2], A. De.[1]

[1] Indian Institute of Technology, Bombay, India
[2] Central School of Nantes, Research Institute in Civil and Mechanical Engineering, Nantes, France
*Corresponding author. Email: rishabhshotri@gmail.com

Abstract

Magnetic pulse welding involves the application of a controlled electromagnetic impulse and consequent high velocity impact between two overlapped parts, which leads to plastic deformation and consolidation between the parts along the interface without melting. The key variables in magnetic pulse welding include a high magnitude discharge energy of damped sinusoidal nature, the coil type and geometry and the materials, thicknesses and geometry of the overlapped metallic sheets. A computer-based coupled electromagnetic and dynamic mechanical analysis of magnetic pulse welding of sheets is presented in this work to provide an insightful understanding of the evolution of joints, which is otherwise intractable for monitoring due to the high speed of the process and the presence of a high electromagnetic field. The computed results show that such a computational process model can serve as a robust design tool for a fundamental understanding as well as for the identification of suitable conditions for achieving a defect-free, reliable joint.

Keywords

Magnetic pulse welding, dissimilar sheets joining, finite element modelling, electromagnetic field - pressure, high velocity impact investigation, high strain rate plastic deformation.

Introduction

Joining of metallic sheets of high strength steel and aluminium alloy is needed for light-weight frames and structures but difficult with conventional arc and laser welding

processes (Karim and Park, 2020). Solid state joining processes that do not involve melting of materials are an option, but only a few are suitable for joining of overlapped sheets (Simar et al., 2017, Zhang et al., 2011).

Magnetic pulse welding (MPW) process realizes a controlled impact and plastic deformation that progresses along the interface of overlapped parts under the application of a short-duration intense electromagnetic (EM) impulse (Faes et al., 2020, Wang et al., 2021). The top part is referred to as the flyer and the bottom part is referred to as the target. The impact at a certain angle and velocity of the flyer onto the target sheet causes plastic deformation at a high strain rate and consolidation along the interface. (Khalil et al., 2020). The impact between the overlapped sheets at a certain range of oblique angles promotes the formation of a jet that aid to rupture and cleaning of the surface impurities, and the joint along the interface of the sheets (Drehmann et al., 2021, Zhang et al., 2021). Computer-based process simulation models showed an ability to provide an insightful understanding of the progressive growth of the joint for MPW of tubes (Shotri et al., 2019). Similar studies for the MPW of sheets are rare and currently evolving.

The primary process variables in MPW include the discharge energy, coil geometry and the coil sheet assembly, which includes the gap between coil and flyer, and the standoff distance between the flyer and the target (Psyk et al., 2017, Kore et al., 2007). The type of material and design of the coil design influences the MPW process and the quality of joint significantly (Itoi et al., 2019, Sarvari et al., 2019, Deng et al., 2018). A variation in the discharge energy results in significant variations in the EM field and consequent EM pressure on the flyer and impact velocity of the flyer. The standoff distance between the flyer and the target influences the impact velocity of the flyer. For example, Deng et al. (2018) reported an increase in the impact velocity from 240 to 300 m/s for standoff distance from 1.25 to 2 mm for MPW of 1 mm thick AA1060 flyer and SS304 target sheets. The foregoing studies shows that MPW is a promising technology for the joining of overlapped sheets. However, the inherent phenomena of the process need an insightful understanding for its adoption towards the larger commercial application. An attempt is made in the present work to develop a coupled analysis of the electromagnetic field and pressure distribution on the flyer, and the resulting progress of the impact velocity and plastic deformation along the interface of overlapped sheets and a focused set of experimental investigations.

Theoretical formulation

The EM analysis is conducted using the Maxwell's governing (diffusion) equations (Chari and Salon, 2000).

$$\frac{1}{\mu\sigma}\nabla^2 \mathbf{H} = \frac{\partial \mathbf{H}}{\partial t} \tag{1}$$

where, H is the EM field intensity vector, μ and σ are the magnetic permeability and electrical conductivity of the elements in the solution domain, considered for the EM analysis. A damped sinusoidal electrical discharge current is provided as the input to the EM analysis (Deng et al., 2018). The computed EM field and induced current density are used to estimate the EM force distribution as follows:

$$F = J \times B \tag{2}$$

The EM pressure on the flyer is calculated further from the estimated EM force (Faes et al., 2020, Nassiri et al., 2015) as follows:

$$p = \int_0^\delta \mathbf{F} dt = \int_0^\delta \mu_r \mu_0 \mathbf{H} \frac{\partial \mathbf{H}}{\partial r} dt = \frac{1}{2} \mu_r \mu_0 (H_s^2 - H_p^2) \tag{3}$$

where F is the EM (Lorentz) force and μ_r, μ_0 are the relative permeability of flyer and air (utilized to model unfilled area of isotropic and homogeneous solution domain), and H_s and H_p are the magnetic fields at the coil – flyer gap and at the skin depth.

The computed EM pressure is provided as an input for the dynamic mechanical analysis which follows the governing relation of equilibrium of momentum (Nassiri et al., 2015) as follows:

$$\ddot{x}_i = F_i / m + b_i \tag{4}$$

where m and b_i represent the mass and initial acceleration of the flyer.

The numerical modelling has considered the solid tetrahedral elements with nodal current density vector as input and EM field as the degree of freedom for the EM analysis, and the solid hexahedral elements which can undertake rate-dependent viscoplastic deformation behaviour for the dynamic mechanical analysis.

Materials and methods

MPW of AA5182 aluminium alloy flyer and DC04 steel target sheets is investigated with a flat O – shaped Cu-OFHC alloy coil. The O – shaped coil geometry was considered to achieve uniform distribution of EM field and pressure of the flyer (Khalil et al., 2020). The electrical discharge circuit with equivalent inductance (L), resistance (R) and overall capacitance (C) of 0.149 µH, 6 mΩ and 408 µF, respectively, is utilized to achieve a rapid discharge of 10 kJ at a frequency (f) of 20.5 kHz and a decrement rate of *exp (-13442×t)*. The current flow in the coil is monitored with a Rogowski coil setup.

The flyer – target sheets are separated at a standoff distance of 1.2 mm with the help of polyethylene insulator blocks. The dimensions of the coil and the flyer – target sheets are represented in Table 1. Table 2, 3 presents the materials properties of the coil and the sheets that are used for the EM and mechanical analysis. Johnson-Cook constitutive model,

as shown in Eq. (5) is used to consider the dynamic mechanical behavior of the flyer and target sheets.

$$\sigma_f = (A + B\varepsilon^n)(A + C\dot{\varepsilon}^m)(1 - \frac{T - T_t}{T_m - T_r}) \tag{5}$$

where σ_f, ε and $\dot{\varepsilon}$ refer to the flow stress (in MPa), equivalent plastic strain and the equivalent strain rate, respectively, T, Tr and T_m are the current temperature, a reference temperature and the melting temperature, respectively, and A, B, C, n and m are the material constants which are given in Table 4. A Photon Doppler Velocimeter set-up is used to measure the flyer impact velocity. The welded interface is examined after peeling off the flyer from the target.

	Material	Length (mm)	Width (mm)	Thickness (mm)
Coil	Cu-OFHC	80	8	4
Flyer	AA5182	70	110	1.2
Target	DC04 steel	70	110	0.8

Table 1 *Materials and dimensions of the coil and flyer – target sheet*

Relative magnetic permeability, μ	Electrical conductivity, σ (S/m)	Density, ρ (kg/m^3)
0.99	5.8×10^7	8960

Table 2 *Material properties of Cu-OFHC coil (Faes et al., 2020)*

Property	AA5182	DC04 steel
Relative permeability, μ	1.0	B-H curve*
Electrical conductivity, σ (S/m)	1.63×10^7	7.54×10^6
Density, ρ (kg/m^3)	2650	7870
Specific heat, c_p (J/kg/K)	902	470
Young's modulus, E (GPa)	69.6	180
Shear modulus, G (GPa)	26	69.2
Melting temperature, T_m (K)	873	1788

B-H curve for steel is presented as Fig. A1 in Appendix.

Table 3 *Material properties of AA5182 flyer and DC04 steel target (Khalil et al., 2020)*

Material constants	AA5182	DC04 steel
Initial flow stress, A (MPa)	109	162
Hardening constant, B (MPa)	552	598
Strain rate sensitivity, C	0.0012	2.623
Hardening exponent, n	0.4	0.6
Thermal softening coefficient, m	3.19	0.009

Table 4 *Constants for AA5182 flyer and DC04 steel target (for Eq. 5) (Rohatgi et al., 2014, Khalil et al., 2020)*

Results and Discussions

Figure 1a-b shows the computed results of EM field and pressure over AA5182 flyer at the time instant of 11 µs for a discharge energy of 10 kJ. Figure 1a shows a typical O – shaped EM field distribution, which confirms to the shape of the coil. The differential distribution of EM field over the flyer sheet is attributed to the variation in the coil cross-section and the surface area of coil – flyer overlap. The maximum computed EM field is 31 T and found to occur at the center of the flyer sheet, which follows the maximum current density in the coil.
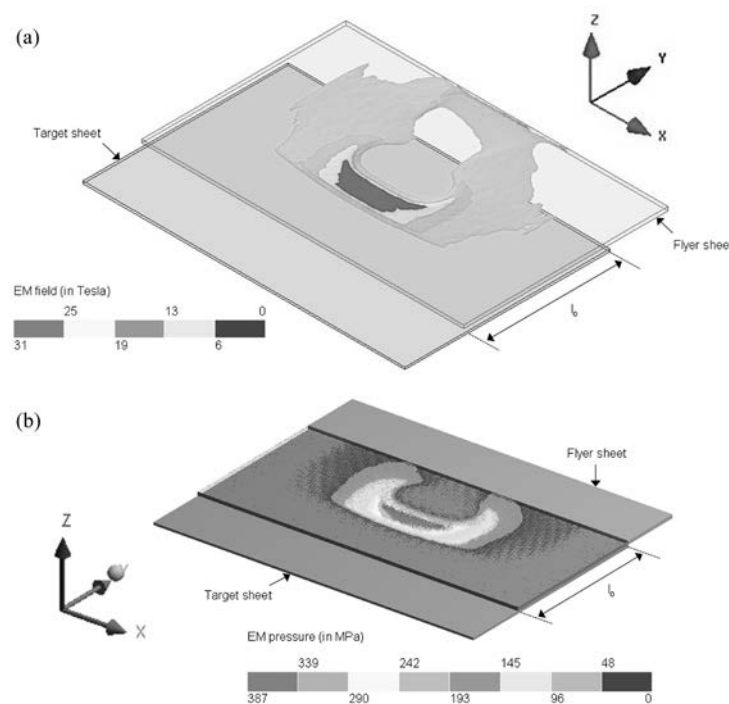

Figure 1. *Computed (a) EM field and (b) EM pressure over the flyer-target sheets assembly for a discharge energy (U) of 10 kJ at 11 µs.*

The EM pressure is computed normal to the flyer surface and follows the EM field distribution. The peak values of EM pressure vary from 339 to 387 MPa. Similar to the coil geometry, both the EM field and pressure distribution tend to elongate in the X – direction and reduce axially outward. As a result, the impact of the flyer and consequent plastic deformation of flyer – target interface proceeds from the center towards the periphery of the sheet.

Figure 2 represents the nature of plastic deformation of the flyer sheet under the applied EM field – pressure at four different time instants for a discharge energy of 10 kJ and a standoff distance of 1.2 mm. Figure 2a shows the initial inward bending of the central region of flyer sheet with maximum deformation of 0.27 mm. After 10 µs, the flyer shows an impact on the target leading to an inward plastic deformation of around 1.2 mm of the flyer – target sheet assembly. The inward deformation of the sheet assembly

increases to around 1.44 mm after an elapse of 12 μs (Fig. 2b), and thereafter slows down with nearly no appreciable inward deformation afterwards till 24 μs (Fig. 2c-d). The computed nature of the progress of plastic deformation of the flyer – target assembly can be explained as follows. The magnitude of the EM pressure reduces after the discharge current reaches its peak value at around 11 μs. Secondly, the impact of the flyer moves outward at rapidly reducing velocity and higher impact angle. Lastly, a steel block is placed to restrict the excessive plastic deformation of the flyer – target assembly. The computed flyer – target contact length in the longitudinal direction is around 69 mm while very little growth in the flyer – target contact is noted in the transverse axis direction, which is attributed to the nature of the EM field and pressure distribution as a result of the shape of the coil.
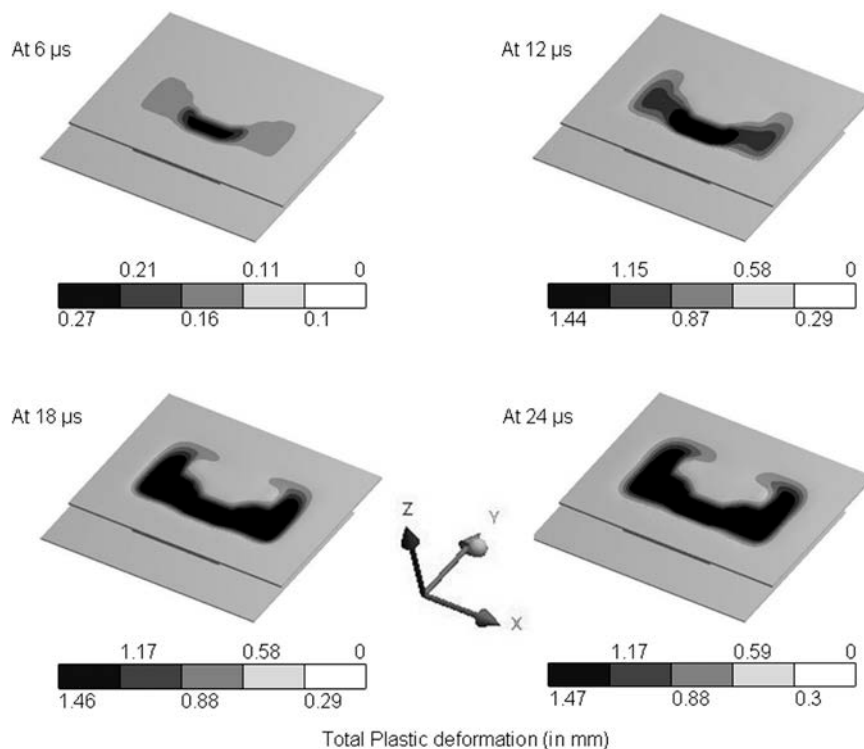

Total Plastic deformation (in mm)

Figure 2. Computed plastic deformation of overlapped sheets assembly for a discharge energy (U) of 10 kJ and a standoff distance (s) of 1.2 mm.

Figure 3 shows the computed flyer impact angle and impact velocity as a function of time. The initial contact is obtained at around 10 μs when the flyer meets the target at an impact velocity of 4.15e5 mm/s and at an impact angle of 1.51°. Subsequent impact of the flyer on the target from 12 to 17 μs occurs at reduced velocities and higher impact angle as shown in Figure 3. The reducing impact velocity and increasing impact angle with time are attributed to rapidly reducing EM pressure, the shift of the flyer impact and inward deformation outward of the flyer-target assembly. The corresponding experimentally measured flyer impact velocity equals to 3.53e5 mm/s. The disparity in the computed and the measured peak flyer impact velocities was observed and is attributed to the simplified

assumptions of the high strain rate behaviour of the metallic sheets for the dynamic mechanical analysis (Haiping et al., 2009).
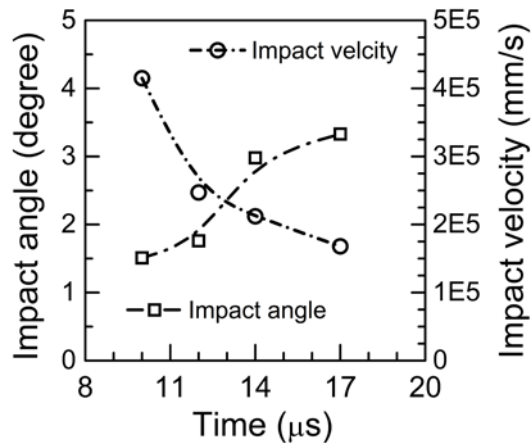

Figure 3. *Computed flyer impact angle and impact velocity as a function of time for a discharge energy (U) of 10 kJ and a standoff distance of 1.2 mm.*

Conclusions

A computational analysis of MPW of AA5182 flyer and DC04 steel target sheets is presented with an overview of the involved electromagnetics and impact dynamic of the process. The analysis is utilized to examine the nature and distribution of the EM field, pressure, impact angle, velocity and resulted plastic deformation as a function of time. The computed results affirm the process parameters for a reasonable MPW weld. The results show the EM field and pressure, and the nature of progress of the impact phenomena to be sensitive and firmly guided by the coil geometry. The computed results further show that the high strain rate deformation of the flyer-target assembly and its rapid progress with time are very important for an insightful understanding of the evolution of the solid-state joint in the MPW process. For the conditions considered here, the computed results indicated that the MPW of overlapped AA5182 and DC04 steel sheets can be realized with an O-shaped coil for a discharge energy of 10 kJ although a more detailed analysis is needed to identify the suitable range of standoff distance and overlapped length of the sheets to produce defect free joints in a reliable manner.

References

Chari, M., V., K., Salon, S., J., 2000. Numerical method in electromagnetic. Academic Press. San Diego. pp. 1-60.

Drehmann, R., Scheffler, C., Winter, S., Psyk, V., Kräusel, V. and Lampke, T., 2021. Experimental and Numerical Investigations into Magnetic Pulse Welding of

Aluminum Alloy 6016 to Hardened Steel 22MnB5. Journal of Manufacturing and Materials Processing, 5(3), p. 66.

Deng, F., Cao, Q., Han, X. and Li, L., 2018. Electromagnetic pulse spot welding of aluminum to stainless steel sheets with a field shaper. The International Journal of Advanced Manufacturing Technology, 98(5), pp. 1903-1911.

Faes, K., Shotri, R. and De, A., 2020. Probing magnetic pulse welding of thin-walled tubes. Journal of Manufacturing and Materials Processing, 4(4), p. 118.

Haiping, Y.U., Chunfeng, L.I. and Jianghua, D.E.N.G., 2009. Sequential coupling simulation for electromagnetic–mechanical tube compression by finite element analysis. journal of materials processing technology, 209(2), pp.707-713.

Itoi, T., Inoue, S., Nakamura, K., Kitta, S. and Okagawa, K., 2019. Lap joint of 6061 aluminum alloy sheet and DP590 steel sheet by magnetic pulse welding and characterization of its interfacial microstructure. Materials Transactions, 60(1), pp. 121-129.

Karim, M.A., Park, Y. D., 2020. A review on welding of dissimilar metals in car body manufacturing, Journal of Welding and Joining. 38(1), pp. 8-23.

Khalil, C., Marya, S. and Racineux, G., 2020. Magnetic pulse welding and spot welding with improved coil efficiency—Application for dissimilar welding of automotive metal alloys. Journal of Manufacturing and Materials Processing, 4(3), p. 69.

Kore, S.D., Date, P.P. and Kulkarni, S.V., 2007. Effect of process parameters on electromagnetic impact welding of aluminum sheets. International journal of impact engineering, 34(8), pp. 1327-1341.

Nassiri, A., Campbell, C., Chini, G. and Kinsey, B., 2015. Analytical model and experimental validation of single turn, axi-symmetric coil for electromagnetic forming and welding. Procedia Manufacturing, 1, pp.814-827.

Psyk, V., Scheffler, C., Linnemann, M. and Landgrebe, D., 2017. Process analysis for magnetic pulse welding of similar and dissimilar material sheet metal joints. Procedia Engineering, 207, pp. 353-358.

Rohatgi, A., Soulami, A., Stephens, E.V., Davies, R.W. and Smith, M.T., 2014. An investigation of enhanced formability in AA5182-O Al during high-rate free-forming at room-temperature: Quantification of deformation history. Journal of Materials Processing Technology, 214(3), pp.722-732.

Sarvari, M., Abdollah-zadeh, A., Naffakh-Moosavy, H. and Rahimi, A., 2019. Investigation of collision surfaces and weld interface in magnetic pulse welding of dissimilar Al/Cu sheets. Journal of Manufacturing Processes, 45, pp. 356-367.

Simar, A., Avettand-Fenoel, M. N., 2017. State of the art about dissimilar metal friction stir welding. Science and Technology of Welding and Joining. 22(5), pp. 389-403.

Shotri, R., Racineux, G. and De, A., 2020. Magnetic pulse welding of metallic tubes–experimental investigation and numerical modelling. Science and Technology of Welding and Joining, 25(4), pp. 273-281.

Wang, C., Liu, Q., Li, G. and Cui, J., 2021. Study on mechanical properties and microstructural feature of magnetic pulse welding joint between Cu and Al sheets.

The International Journal of Advanced Manufacturing Technology, 113(5), pp. 1739-1751.

Zhang, Y., Babu, S.S., Prothe, C., Blakely, M., Kwasegroch, J., LaHa, M. and Daehn, G.S., 2011. Application of high velocity impact welding at varied different length scales. Journal of Materials Processing Technology, 211(5), pp. 944-952.

Zhang, S., Lueg-Althoff, J., Hahn, M., Tekkaya, A.E. and Kinsey, B., 2021. Effect of process parameters on wavy interfacial morphology during magnetic pulse welding. Journal of Manufacturing Science and Engineering, 143(1), p. 011010.
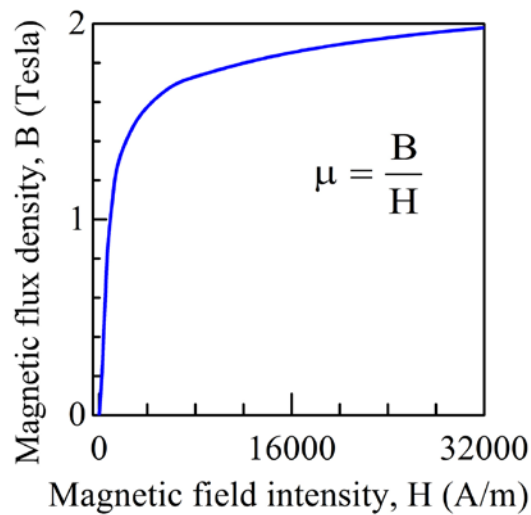
Appendix

Figure A1. *Non-linear B-H curve used to assign magnetic permeability of steel (target)*